Double-Sided Conformable Piezoelectric Force Sensor with Enhanced Performance and Bending Correction

Joseph Faudou, Mohammed Benwadih, Abdelkader Aliane, Christine Revenant, Daniel Grinberg, Minh-quyen Le, Pierre-jean Cottinet

ADVANCED ELECTRONIC MATERIALS Open Access
www.advelectronicmat.de

Double-Sided Conformable Piezoelectric Force Sensor with Enhanced Performance and Bending Correction

Joseph Faudou, Mohammed Benwadih,* Abdelkader Aliane, Christine Revenant, Daniel Grinberg, Minh-Quyen Le, and Pierre-Jean Cottinet*

Flexible piezoelectric devices have gained considerable interest due to their potential for new applications, particularly in wearable technology. However, a significant challenge remains in measuring low forces on nonplanar and deformable surfaces. Indeed, conformability on complex surfaces induces bending stresses in the piezoelectric sensors, interfering with the measurement of compressive force. Yet such measurements can be valuable, especially in medical applications that involve assessing forces on soft tissues. This study presents an innovative highly sensitive conformable sensor based on a thin film of P(VDF-TrFE) copolymer. The selection of the substrate is essential for ensuring the device's conformability, but it is also demonstrated that it can provide a substantial improvement in performance if its Young's modulus is lower than that of the active polymer. The effective piezoelectric charge coefficient $d_{33_{eff}}$ of a sensor on TPU substrate is measured equal to −340 pC.N^{-1}, representing a tenfold increase in the theoretical compression sensitivity of P(VDF-TrFE). Additionally, a double-sided structure to eliminate the contribution of bending in the piezoelectric signal and tackle the challenge of conformability on complex surfaces is developed. Overall, the proposed device shows promising results for measuring low forces applied to soft biological tissues such as skin or heart valve leaflets.

1. Introduction

Conformable piezoelectric force sensors should be able to measure stresses applied to complex surfaces, meaning non-flat and deformable surfaces. This is particularly relevant for medical applications, as biological soft tissues exhibit such characteristics.[1,2]

Piezoelectric devices are usually made of ceramic materials. Piezoceramics offer excellent electromechanical coupling but are rigid and brittle, making them unsuitable for flexible electronics. In addition, there are significant concerns about the biocompatibility of these materials for medical applications.[3,4] However flexible piezoelectric devices are of real interest for wearable applications on the human body,[5–10] to be used as energy harvesters for self-powered devices or as sensors for health monitoring.[11–19] Therefore, those devices are generally made from a piezoelectric polymer film, often based on polyvinylidene fluoride (PVDF). Despite lower electromechanical performance compared to ceramics, polymers are usually cheaper, more flexible, and biocompatible, making them more suitable for the targeted applications.

Piezoelectric polymer films are usually too thin (under 20 µm) to be manipulated on their own. Therefore, PVDF is frequently deposited on a thicker substrate used as a mechanical support for fabrication and the intended use of the device. To some extent, the substrate plays a crucial role in the mechanical properties of the sensor, which in turn affects its sensing performance as well as its conformability. Most of the substrates chosen for flexible thin sensors have a wide range of Young's modulus (denoted Y) comprising relatively rigid but thin materials as polyimide (PI), polyethylene naphthalate (PEN), or polyethylene terephthalate (PET) ($Y \approx 1$–10 GPa), or very soft materials as polydimethylsiloxane (PDMS) or polyurethane (PU) ($Y < 100$ MPa).[20–24]

In this paper, we focus on measuring compressive forces with flexible sensors for medical applications, such as pressure exerted on human skin or contact force between soft biological tissues like leaflets in a cardiac valve. Compressive forces involve the d_{33} longitudinal mode of piezoelectricity, in which the induced stress is along the poling field (i.e., axis 3 in the thickness direction). Measuring stress in this mode is challenging because the

J. Faudou, M. Benwadih
Univ. Grenoble Alpes, CEA, LITEN
Grenoble 38000, France
E-mail: joseph.faudou@cea.fr; mohammed.benwadih@cea.fr
J. Faudou, M.-Q. Le, P.-J. Cottinet
LGEF Laboratory, INSA Lyon, UR682
Villeurbanne 69621, France
A. Aliane
Univ. Grenoble Alpes, CEA, LETI
Grenoble 38000, France
C. Revenant
Univ. Grenoble Alpes, CEA, IRIG
Grenoble 38000, France
D. Grinberg
Department of Cardiac Surgery
"Louis Pradel" Cardiologic Hospital
Bron 69500, France

The ORCID identification number(s) for the author(s) of this article can be found under https://doi.org/10.1002/aelm.202400456

DOI: 10.1002/aelm.202400456

flexibility of a thin piezoelectric film favors bending strain manifested by the d_{31} transverse mode of piezoelectricity, in which the induced stress is along axis 1 (perpendicular to axis 3). Usually in thin films, the bending mode generates a significantly higher electric charge than the compression mode. It is chosen to design highly efficient piezoelectric energy harvesters or highly sensitive sensors.[25–27] Consequently, the bending effect often disturbs the compressive output signal in flexible thin sensors, making it difficult to extract the effective d_{33} through direct compressive force measurement.[28,29] One solution is to allow the initial compressive stress to generate bending in the film and use the induced d_{31} signal to measure the applied force.[30] However, unlike the d_{33} mode, there is no simple relationship between the input force and the output charge under the bending d_{31} mode, except for some specific conditions.[31] Therefore, sensors based on bending operating mode are frequently limited to the application they are designed for.

This study aims to present an innovative, highly sensitive conformable force sensor using the ferroelectric copolymer P(VDF-TrFE). The proposed screen-printed device features a double-sided design and can measure low compressive forces on non-flat, deformable surfaces in various applications, by directly distinguishing between compressive and bending signals, even if they are superimposed. In addition, it is highlighted that a soft thermoplastic polyurethane (TPU) substrate enhances sensing performance while maintaining a linear response between the applied compressive force and the piezoelectric charge. Several studies have already highlighted the fact that the mechanical interaction of a piezoelectric film with a flexible substrate leads to an increase in performance compared with more rigid substrates, thanks to complex deformations involving the d_{31} mode of piezoelectricity.[32,33] However, these studies may lack a physical interpretation and theoretical models to explain the phenomenon and often rely on numerical simulation models to support experimental data. In this work, experimental measurements are supported by an analytical model and finite element (FE) simulations.

The device is based on the principle of a piezoelectric bimorph, where two identical piezoelectric sensors stacked on top of each other either cumulate or cancel out their respective effect. In our case, compressive signals will add up and bending signals will cancel each other out. Therefore, the bimorph concept appears to be an efficient solution to overcome the bending effect in order to extract the useful compressive signal from the sensor output. To the best of our knowledge, this approach is being applied for the first time to soft and conformable force sensors.

Bimorphs have been widely studied, but mostly with piezoelectric ceramics such as lead zirconate titanate (PZT) for actuators or energy harvesters.[34–36] However, all these devices are too rigid for conformable applications.

Some flexible sensors with two distinct piezoelectric layers have already been used to distinguish various mechanical stresses or enhance performance. For instance, Hong et al. presented two piezoelectric layers with different kirigami structures to estimate bending direction, but the compressive load was ignored.[37] Moreover, Lin et al. separated two piezoelectric layers with a thick PDMS layer to differentiate between bending, compression, and shear. However, in their device, compressive force actually generates bending in the piezoelectric films and their concept is not suitable when both bending and compressive stresses are simultaneously applied to the device.[28] Alternatively, zinc oxide (ZnO) nanostructures grown on both sides of a conductive layer have been used to form double-sided sensors with increased piezoelectric performance and the ability to detect bending direction.[38–40]

None of these studies precisely meets our requirements. This is the main reason why this paper takes a particular look at the bimorph structure capable of measuring compressive forces exerted on complex surfaces (deformable and curved). Technical challenges related to fabrication and use followed by methods and solutions are discussed, confirming the feasibility of the piezoelectric sensor for promising medical applications.

2. Materials, Design and Fabrication Process

2.1. Materials Selection

In this study, the ferroelectric copolymer P(VDF-TrFE) (80/20 proportion, from Arkema Piezotech) was chosen to fabricate the active sensing element. Thanks to its good piezoelectric response, ease of processing, good flexibility and ability to be used in the form of very thin films, P(VDF-TrFE) is considered the most mature flexible piezoelectric material and has been widely used, especially in medical fields.[41–46] Although the use of composites or particular structures and interfaces can improve its performance,[47–51] we decided to fabricate the thin-film sensor with pure P(VDF-TrFE) due to its simplicity and reproducibility (no agglomeration issues as in the case of the composites) while maintaining its good efficiency.[52] For flexible electrodes, the conductive polymer poly(3,4-ethylenedioxythiophene) polystyrene sulfonate (PEDOT:PSS, manufactured by Heraeus) was chosen as it is flexible, easy to process and creates good electrical contacts when interfaced with P(VDF-TrFE).[53–55]

The substrate was selected based on its mechanical properties to obtain a conformable device whose bending stiffness (denoted D, an indicator of conformability) is determined as:

$$D = \frac{Yh^3}{12\,(1-\nu^2)} \tag{1}$$

with Y as Young's modulus, h the thickness, and ν the Poisson's ratio of the sample. Our previous work has demonstrated the ability to print piezoelectric sensors on various substrates with a wide range of bending stiffness.[56] Based on experience, it was estimated that a conformable substrate should have a bending stiffness approximately within the interval $[10^{-6}; 10^{-4}]$ N.m. Beyond the upper value, a substrate is too rigid to properly conform to the shape of a surface with a high curvature (radius of curvature down to 1 cm). On the other hand, an excessively soft substrate could make it difficult to process and impractical in application. Obviously, the bending stiffness range may vary depending on the intended application. In fact, the constraint on stiffness eliminates a large number of substrates used in flexible electronics, such as rigid polymers like PI, PEN, or PET with a thickness greater than 100 µm.

According to Equation (1), the desired bending stiffness can be achieved by selecting a substrate with a low Young's modulus or one with low thickness. In the following study, a flexible

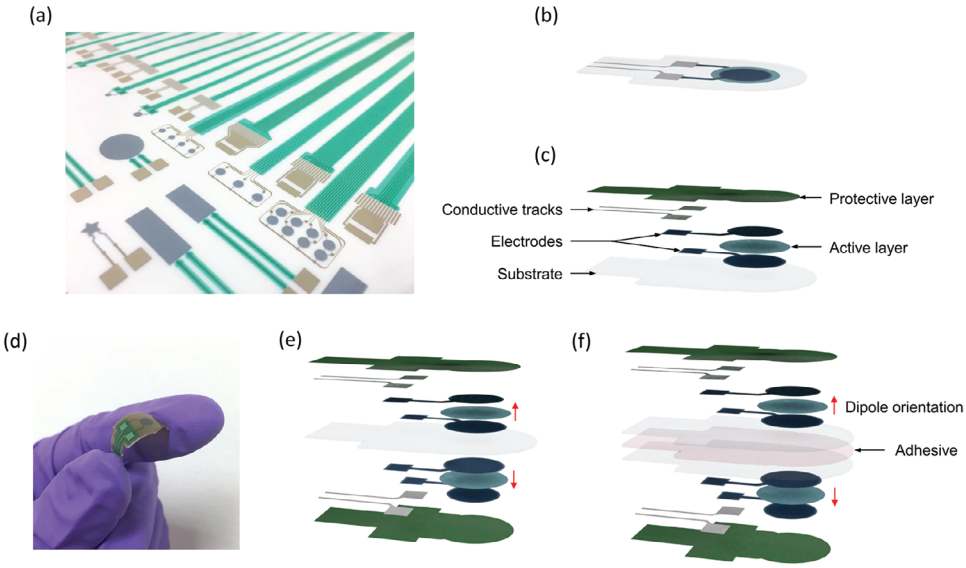

Figure 1. Structure and design of the piezoelectric sensors: a) image of multiple sensors printed on a TPU substrate; b) design of a unit sensor; c) layer stacking within a unit sensor; d) image of a conformable double-sided sensor on TPU substrate; layer stacking of a piezoelectric bimorph e) printed on both sides of a single substrate; or f) fabricated by bonding two substrates.

Table 1. Mechanical properties of substrates. Young's modulus is measured by nanoindentation.

Substrate	Young's modulus [GPa]	Thickness [μm]	Poisson's ratio	Bending stiffness [N.m]
TPU	0.05	100	0.4	5×10^{-6}
PI	6	50	0.35	7.1×10^{-5}

TPU substrate with low Young's modulus (Intexar TE-11C from DuPont) was chosen for comparison with a more rigid PI substrate with lower thickness (Upilex from UBE). Both selected substrates are presented by their manufacturers as suitable for printing manufacturing techniques. Their mechanical properties are reported in **Table 1**. These are the most relevant physical parameters to be identified for the rest of the study.

As shown, the bending stiffness of these materials is within the interval set for the conformable substrate. As stiffness increases with substrate thickness, this parameter has been minimized to achieve the desired conformability, but without being too thin, to avoid making the substrate too difficult to handle. The objective is to assess the influence of the substrate material property (i.e., Young's modulus Y) and its dimension (i.e., the thickness h) on the conformability and performance of the device. From a manufacturing perspective, PI was easier to process thanks to its good resistance to solvents, lower roughness, and reduced thermal expansion. As TPU is too soft to be processable alone, it was delivered with a liner to reinforce its structure.

2.2. Printing Process

To fabricate the piezoelectric sensors, screen-printing additive manufacturing was employed for its maturity, simplicity, low cost, and speed, making it scalable for industrial use in organic electronics.[57–60] **Figure 1a** illustrates several sensors of different sizes and patterns, simultaneously printed on a 38×32 cm^2 substrate. The sensors were printed individually or in arrays for mapping the force distribution of a surface. As shown in Figure 1b,c, each unit sensor is composed of several stacked layers: a substrate, an active P(VDF-TrFE) copolymer (3 μm thickness) sandwiched between the top and bottom electrodes made of PEDOT:PSS (1 μm thickness), and a non-active P(VDF-TrFE) layer as a protective cover (3 μm thickness). Conductive tracks were printed with silver ink to efficiently transmit the sensor signal to the interface electronics. To avoid any parasitic capacitance effect that could impact the force measurement of the arrayed sensors, the conductive tracks must fulfill the design rules reported in previous work.[61]

The thickness of each printed layer was minimized to avoid drastically increasing the stiffness of the device, while ensuring that they fulfilled their functional role properly. This was particularly important for the piezoelectric active layer, as a reduction in its thickness does not decrease its sensitivity to compression, but it does reduce its response to bending, which must be completely eliminated.

The printing process took place in a clean room using an EKRA screen printer from IPP Electronics. Before printing, substrates were annealed at 135 °C for 20 min to trigger the thermal strains that would occur during the thermal evaporation of ink solvent, which could cause misalignment between layers. This was especially necessary for the TPU substrate.

First, the PEDOT:PSS bottom electrode was printed via a screen with a 325-24 (threads per centimeter - thread thickness in μm) stainless steel mesh (from Koenen) and then annealed at 110 °C for 10 min to evaporate the solvent and initiate cross-linking. The final electrode layer is ≈1 μm thick. Second, two printing passes of the active P(VDF-TrFE) copolymer were conducted with a 100-40 polyester mesh, followed by a 3 min annealing under vacuum at 150 °C. Using two printing passes instead

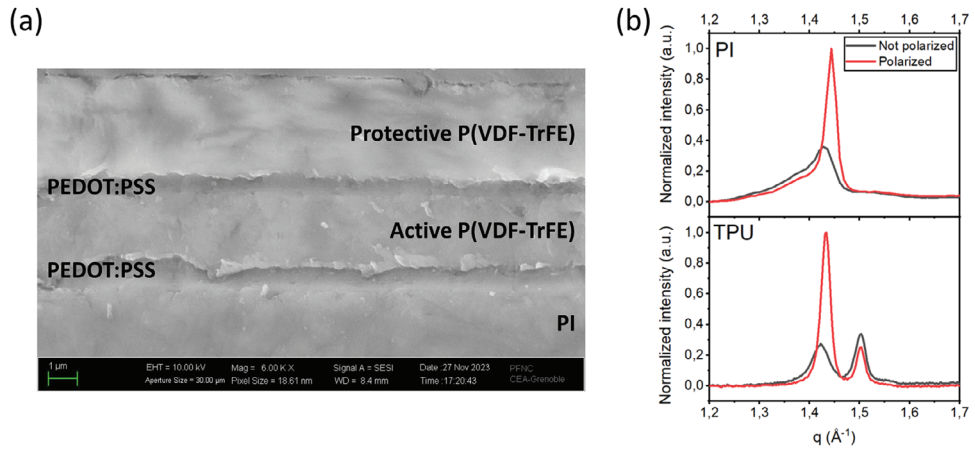

Figure 2. Sensor microstructure analysis: a) SEM image of the cross-section of a sensor on a PI substrate; b) XRD of active P(VDF-TrFE) (with baseline correction and different types of the substrate) before and after polarization.

of one is crucial to minimize defects of the sensor's surface as well as to obtain a uniform final layer of 3 µm thickness. This was the thinnest thickness that could be achieved while maintaining a good yield, since the size of dust particles is typically around 1 µm. Next, the PEDOT:PSS top electrode was printed on the copolymer layer in a similar manner as the bottom one. Since PEDOT:PSS is not conductive enough to efficiently transmit the piezoelectric signal to the interface electronics, particularly on long distances, silver ink (purchased from Taiyo Ink) was chosen for conductive tracks. It was actually the most challenging layer in terms of resolution, as it needed patterns down to 100 µm to connect all the piezoelectric sensors in a dense array. Thus, the conductive tracks were printed with a 400-18 stainless steel mesh and annealed for 10 min at 110 °C. Afterward, an encapsulation layer made of a non-active copolymer was printed with a 165-50 stainless steel mesh on top to protect the sensor from the external environment, especially as the PEDOT:PSS electrode is sensitive to humidity.[62] The protection layer was thermally treated under the same conditions as for the active P(VDF-TrFE) layer. Finally, the whole sample was annealed for 20 min at 135 °C to complete the cross-linking of PEDOT:PSS electrodes and improve their conductivity.

Regarding the fabrication of piezoelectric bimorphs (Figure 1d), there are several ways to proceed. Correct alignment of the two sensors in a face-to-face configuration is crucial to obtain a symmetrical signal during application. By using screens with symmetric patterns, each layer can be printed on both sides of one substrate, perfectly superimposing the patterns (Figure 1e). This method is feasible with the PI substrate, but impractical with the TPU substrate because of its liner.

Therefore, for TPU substrate, two identical sensors were stacked together by bonding their own substrates (Figure 1f) with a double-sided adhesive layer made of a 25 µm thick PI substrate with water-resistant VHB adhesive from 3 M on both sides. Those sensors were manually aligned along their contour that was cut by a high-precision laser. Compared to the "single-substrate" method (Figure 1e), the "double-substrate" one (Figure 1f) leads to an increase in the device thickness due to an addition of the adhesive and one more substrate layer. For instance, a double-sided piezoelectric device made of TPU has a total thickness of ≈350 µm, resulting in higher bending stiffness of $D \approx 2 \times 10^{-4}$ N.m (estimated using the calculation method of the bending stiffness for composite materials),[63] slightly exceeding the target set earlier for conformability. In addition, an increase in the distance between the two piezoelectric layers also increases the device's sensitivity to bending, which should ideally be avoided.

To activate the sensing response, the active P(VDF-TrFE) layer was subjected to an electric field of ≈100–130 V µm^{-1} using a Multiferroic ferroelectric tester (Radiant Technologies). The dipoles of the β crystalline phase are expected to align along the poling field, which is responsible for the piezoelectric properties.[64] After the polarization phase, the two sensors of a piezoelectric bimorph exhibit opposite dipole orientation as illustrated in Figure 1e,f.

To validate the efficiency of the printing process, Scanning Electron Microscopy (SEM) of the screen-printed layers was performed using a NVision 40 from ZEISS. As illustrated in **Figure 2a**, the microstructure of a sensor printed on PI shows good layer homogeneity with few defects, and a good interface between layers, with no signs of delamination. Additionally, X-ray diffraction (XRD) was carried out using a D8 diffractometer (Bruker), in θ-2θ reflection geometry with Cu Kα radiation. The test was conducted on the active piezoelectric layer, before and after polarization with a focus on the β-phase peak at scattering vector $q = 1.43$ Å^{-1}. Since PI and TPU substrates also produce signals in this area, the analysis was performed on thicker P(VDF-TrFE) active films (≈6 µm) without a protective layer to obtain a more intense β peak, so easier for visualization. The results presented in Figure 2b show that for both selected substrates, electrical polarization effectively activates the piezoelectric properties of the copolymer. As observed, the β phase exhibits higher peak intensity, and the size of the crystal domains is doubled from ≈13–26 nm, as evidenced by a narrower peak.

3. Results and Discussion

3.1. Electrical Characterizations

Multiple electrical characterizations were performed to validate the sensors' performance after fabrication on PI and TPU

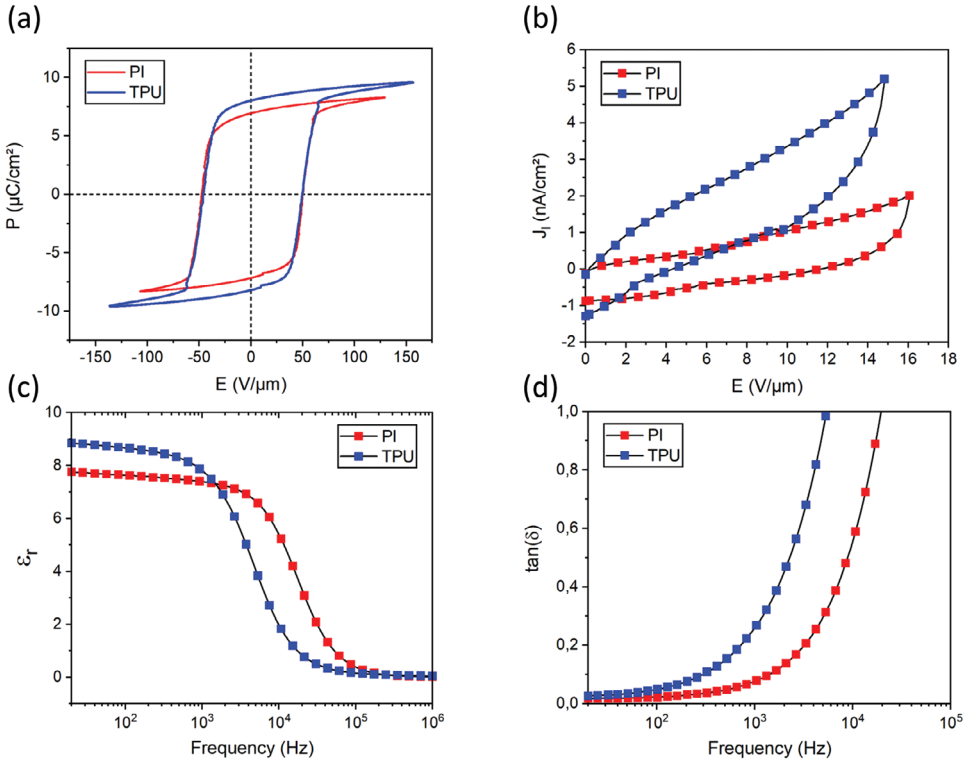

Figure 3. Electrical characterizations of two piezoelectric sensors with identical geometry on TPU and PI substrates: a) hysteresis polarization cycles P-versus-E; b) leakage current density; c) relative permittivity; d) dielectric loss.

substrates. The hysteresis curves P-versus-E displayed in **Figure 3a**, where P and E denote the induced polarization (or charge displacement) and the input electric field respectively, reflect a typical ferroelectric behavior of the active layer. The remnant polarization is high and close to the maximum theoretical value for the P(VDF-TrFE) copolymer,[65] together with a significant hysteresis area that ensures a good polarization process. The I–V curves shown in Figure 3b were measured with a Precision Current-Voltage Analyzer (Keysight), confirming low leakage currents of the sensing device. The capacitance and resistance of the devices were measured with an E4980A RLC meter (Agilent) over a large frequency range, from which were calculated the relative permittivity (the so-called dielectric constant ε_r, see Figure 3c) and the loss tangents (denoted tanδ, see Figure 3d) of the active layer. As expected in Figure 3c, ε_r was found equal to 9 and stable at low frequencies. Under the same operating condition that is of high interest for medical use (i.e., below 20 Hz), the tanδ loss is low enough to neglect the current leakage principally due to the conduction effect (Figure 3d).[66] Overall, the electrical characterizations demonstrate the good performance of the fabricated devices. **Table 2** summarizes the average and standard deviation values determined from five sensors for each type of substrate.

Slight differences can be observed between samples made with PI and TPU substrates. The better processability of PI leads to fewer defects in the P(VDF-TrFE) active layer, which explains the lower leakage current and higher cut-off frequency. Moreover, different remnant polarization and relative permittivity might reflect somewhat different semi-crystalline microstructures of the P(VDF-TrFE) depending on the substrate. However, these differences are not sufficient to favor the use of one substrate over the other.

Electrical characterizations were also performed to verify that two sensors in a piezoelectric bimorph have similar characteristics. **Table 3** shows the average differences between two sensors of a bimorph for various parameters.

3.2. Effective d_{33} Measurements

In practice, a Kistler 5015 charge amplifier was used to measure the piezoelectric response of a sensor during mechanical loading. All tests were performed at a frequency of 1 Hz or lower. The raw

Table 2. Electrical properties of piezoelectric sensors on PI and TPU substrates (N = 5).

Substrate	Maximum polarization P_{max} [μC.cm^{-2}]	Remnant polarization P_r [μC.cm^{-2}]	Relative permittivity ε_r @20 Hz	Dielectric loss tanδ @20 Hz	Leakage current J_l [nA.cm^{-2}] @10 V/μm
PI	9.0 ± 0.5	7.5 ± 0.6	8.9 ± 0.5	0.026 ± 0.012	1.4 ± 0.6
TPU	9.7 ± 0.5	8.2 ± 0.3	9.4 ± 1.1	0.034 ± 0.014	3.5 ± 0.2

Table 3. Average differences between two sensors of a bimorph (in %).

Substrate	Number of tested bimorphs	Maximum polarization P_{max}	Remnant polarization P_r	Coercitive voltage U_c	Relative permittivity ε_r @20 Hz	Dielectric loss tanδ @20 Hz	Leakage current J_l @10 V/µm
PI	10	2.4%	2.4%	4.2%	5.2%	6%	33%
TPU	9	4%	5.2%	12%	11%	19%	21%

Note that the discrepancy in coercive voltage mainly reflects a variation in the thickness of the P(VDF-TrFE) active layer. Overall, there are only slight differences between the two sensors of a bimorph. The variations are generally greater for the TPU substrate, providing further evidence that the PI substrate leads to better uniformity throughout the fabrication process. The two parameters for which the differences between sensors seem to be the most significant (i.e., dielectric loss tanδ and leakage current) are of little importance as they are, in all cases, very low and guarantee good sensor performance. Indeed, the dielectric tanδ is below 0.05 and the leakage current is less than 30 nA.cm^{-2}. The highest leakage current measured was 0.005 µA (for a 1.2 cm^2 sensor), which remains negligible compared to the threshold that is considered dangerous to patient (≈50 µA) according to medical standards (IEC 60601-1).

electric charge output was low-pass filtered at 10 Hz to reduce undesired perturbations from the 50 Hz power supply. Overall, it can be considered that the electric charge measured was consistent with the theory of piezoelectricity. To limit measurement noise and triboelectric charge upon contact with the sensor, the top electrode was always connected to the ground of the charge amplifier.[67]

Effective piezoelectric coefficient $d_{33_{eff}}$ was measured using a homemade pressure testbench illustrated in **Figure** 4a. To obtain a clean compression signal (see Figure S1, Supporting Information), the sensor was fixed with weak double-sided adhesive (silicone rubber 9030 W from Teraoka) to a flat glass support to prevent bending deformation. A flat indenter, whose surface area was larger than the effective sensor surface (defined as the surface of the electrodes), and perfectly parallel to it, was connected to a micrometric motor capable of exerting a compression load between 0.02 and 10 N (i.e., in the range of interest for medical applications). A force sensor implemented above the indenter allowed us to measure the effective force by considering the surface ratio between the sensor and the indenter. Since the piezoelectric sensor has a small surface area (with a diameter of 2.3 or 3.2 mm), the compressive force exerted on it (denoted F) can be considered uniform. Measurement uncertainty on this testbench is estimated at ≈10% (Figure S2, Supporting Information).

Therefore, the piezoelectric response measured by the charge amplifier can be expressed as follows:[68]

$$Q = -d_{33_{eff}} \times F \tag{2}$$

with Q the electric charge (C) generated by the piezoelectric sensor, F the applied compressive force (N), and $d_{33_{eff}}$ (C.N^{-1}) reflects the sensor sensitivity that depends on the electromechanical coupling of P(VDF-TrFE) copolymer. Figure 4b shows the time evolution of the input force and output electric charge (i.e., perfectly in phase as indicated in Equation 2) of sensors made with TPU or PI substrates with a surface area of 4.15 mm^2. Excellent linearity of the piezoelectric response was achieved (Figure 4c,d), regardless of the selected substrate. Surprisingly, the TPU sample has a $d_{33_{eff}}$ of ≈−340 pC.N^{-1}, which is tenfold higher than that of the PI sample, with which $d_{33_{eff}}$ is close to the theoretical value of the P(VDF-TrFE) copolymer, i.e., ≈−30 pC.N^{-1}.[69] In fact, a much better signal-to-noise ratio was obtained with the TPU sample

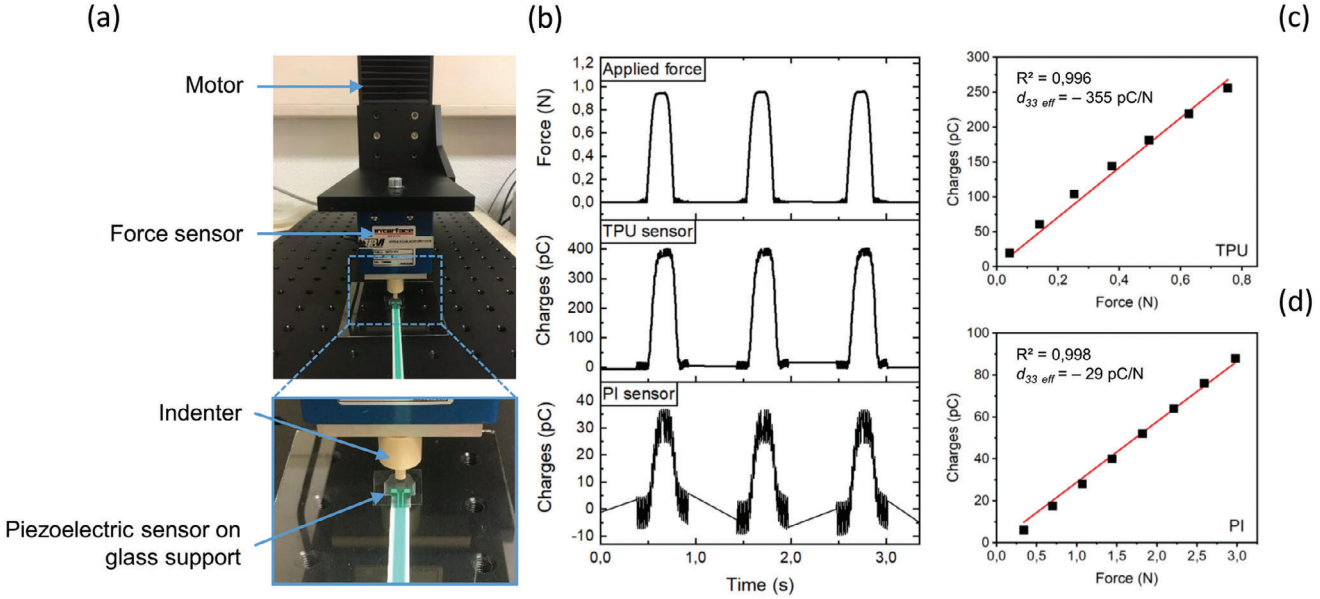

Figure 4. Experimental setup of the piezoelectric characterization: a) image of the testbench; b) response of TPU and PI sensors to compressive loads; linearity of charge-versus-force curve leads to an estimation of $d_{33_{eff}}$ for sensors printed on c) TPU substrate and d) PI substrate.

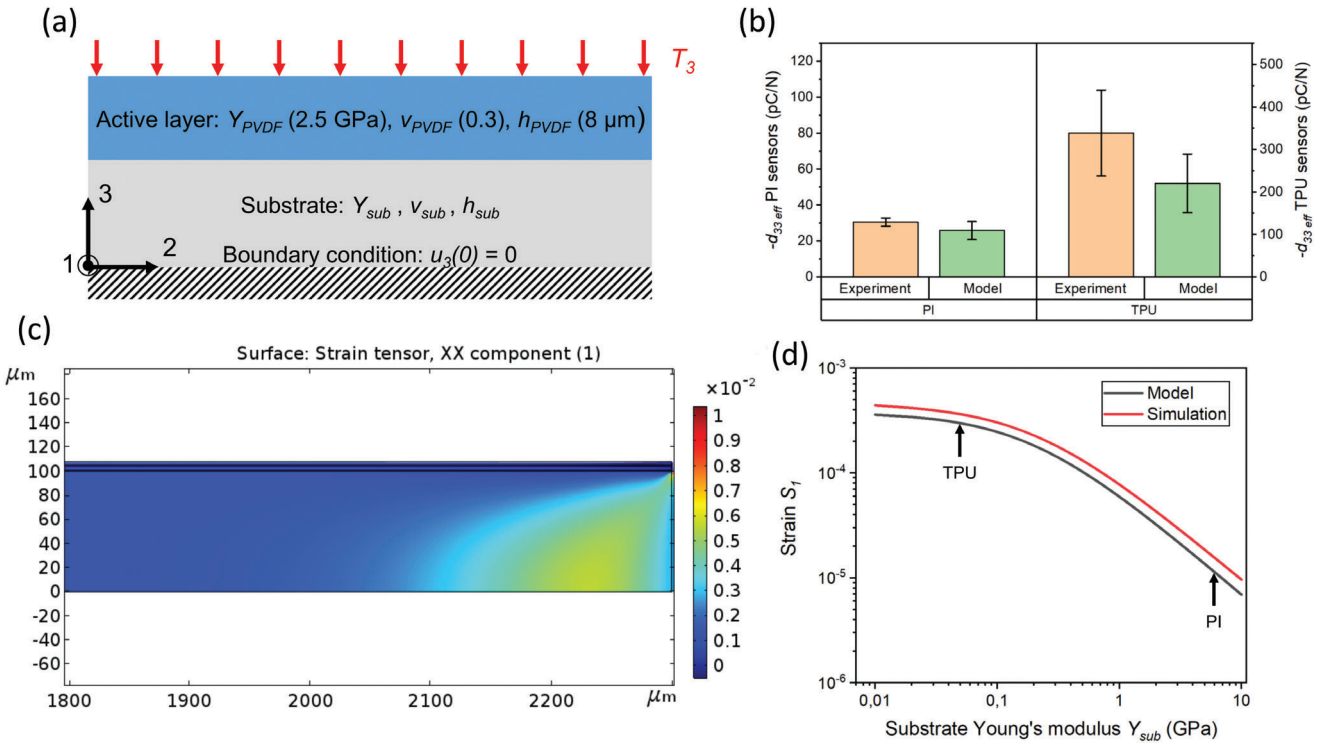

Figure 5. Comparison among experiments, analytical model, and numerical simulation: a) model and simulation configuration of the sensor; b) comparison of $d_{33_{eff}}$ between experiments and analytical model; c) in-plane strain in simulation from the middle to one edge of the device; d) mechanical comparison between analytical model and simulation.

(Figure 4b) enabling the measurement of extremely low forces of less than 0.05 N (Figure 4c).

Obviously, the small discrepancies observed in the electrical and spectroscopic characterizations of these samples (cf. Figures 2 and 3) could not be the primary cause of such a large gap in piezoelectric sensitivity. This performance gap is likely due to significant differences in the mechanical properties of the substrates, which are next thoroughly investigated using analytical models.

3.3. Analytical and Numerical Models

Theoretically, the relationship between the applied stress (denoted T_i, in N.m^{-2}, where the subscript $i = 1, 2, 3$ represents the direction) and the induced electric charge displacement (denoted D_i, in C.m^{-2}) of the P(VDF-TrFE) layer is given by:[68]

$$D_3 = d_{31} \cdot (T_1 + T_2) + d_{33} \cdot T_3 \quad (3)$$

3 being the thickness direction, 1 and 2 the directions in the plane of the sensor, and d_{ij} the piezoelectric coefficients (C.N^{-1}). Usually, for compressive stress applied in direction 3, it can be assumed that $T_1 = T_2 = 0$ and therefore $d_{33_{eff}} = d_{33}$. However, this assumption does not hold when considering the mechanical interaction between the substrate and the piezoelectric layer. This mechanism of interaction seems to be the origin of the significant difference in the effective d_{33} observed between PI and TPU substrates.

Indeed, compressive stress creates in-plane Poisson strain in the substrate which generates in-plane stress in the piezoelectric layer, resulting in an additional d_{31} contribution to the effective d_{33}. A softer substrate will induce in-plane traction in the piezoelectric material while a stiffer substrate will induce in-plane compression. Since the d_{31} and d_{33} coefficients have opposite signs, the piezoelectric charge generated by compression in direction 3 is added to that generated by in-plane traction in directions 1 and 2. This may explain the increase in performance observed with the softer TPU substrate compared with the more rigid PI substrate.

Torah et al.proposed a model applicable to very stiff substrates, where the mechanical influence of the piezoelectric film on the substrate can be ignored.[70] In contrast, Chakhchaoui et al. tried to explain the exact opposite for a much softer substrate.[33] The model developed in this study aims to be valid in all situations.

In this study, the device is modeled as an active piezoelectric layer on top of a substrate layer, subjected to a uniform compressive stress T_3. Nanoindentation measurements indicate that P(VDF-TrFE) and PEDOT:PSS have similar mechanical properties. Consequently, both electrodes and encapsulation are integrated with the active copolymer to form a unique active layer, with a total thickness of 8 µm, Young's modulus Y_p of 2.5 GPa, and a Poisson's ratio v_p of 0.3. **Figure 5a** illustrates the configuration used for the model.

The materials are assumed to be isotropic, implying that $T_1 = T_2 = T$ and $S_1 = S_2 = S$ where S refers to the strain in the active

layer. Hooke's law is used to estimate the in-plane stress T in the piezoelectric layer:

$$S = \frac{1-\nu_p}{Y_p}.T - \frac{\nu_p}{Y_p}.T_3 \tag{4}$$

During the compressive test, the in-plane strain S is assumed to be identical in both the substrate and the active layer, while the in-plane stress within the device is globally null. Thus, the following equation holds:

$$S = -\frac{\nu_{eq}}{Y_{eq}}.T_3 \tag{5}$$

where Y_{eq} and ν_{eq} are respectively the Young's modulus in direction 3 and the Poisson's ratio of the equivalent material composed of both substrate and active layer. Equations (4) and (5) yield the following result:

$$T = -\frac{Y_p}{1-\nu_p}\left(\frac{\nu_{eq}}{Y_{eq}} - \frac{\nu_p}{Y_p}\right).T_3 \tag{6}$$

Substituting Equation (6) into Equation (3) results in:

$$D_3 = \left(d_{33} - 2d_{31}\frac{Y_p}{1-\nu_p}\left(\frac{\nu_{eq}}{Y_{eq}} - \frac{\nu_p}{Y_p}\right)\right).T_3 \tag{7}$$

To calculate Y_{eq} and ν_{eq}, Y. Luo proposed an improved version of the Reuss formula for composite materials under iso-strain conditions, by incorporating the effect of Poisson deformation:[71]

$$Y_{eq} = \frac{Y_p Y_{sub}\left[h_p\left(1-\nu_{sub}\right)Y_p + h_{sub}\left(1-\nu_p\right)Y_{sub}\right]\left[h_{sub}+h_p\right]}{Y_p Y_{sub}\left[h_p^2\left(1-\nu_{sub}\right)+h_{sub}^2\left(1-\nu_p\right)\right] + h_p h_{sub}\left[\left(1+\nu_{sub}\right)\left(1-2\nu_{sub}\right)Y_p^2 + 4\nu_p\nu_{sub}Y_pY_{sub} + \left(1+\nu_p\right)\left(1-2\nu_p\right)Y_{sub}^2\right]} \tag{8}$$

$$\nu_{eq} = \frac{Y_p Y_{sub}\left[h_p\left(1-\nu_{sub}\right)\nu_p + h_{sub}\left(1-\nu_p\right)\nu_{sub}\right]\left[h_{sub}+h_p\right]}{Y_p Y_{sub}\left[h_p^2\left(1-\nu_{sub}\right)+h_{sub}^2\left(1-\nu_p\right)\right] + h_p h_{sub}\left[\left(1+\nu_{sub}\right)\left(1-2\nu_{sub}\right)Y_p^2 + 4\nu_p\nu_{sub}Y_pY_{sub} + \left(1+\nu_p\right)\left(1-2\nu_p\right)Y_{sub}^2\right]} \tag{9}$$

where Y_{sub} and ν_{sub} are the mechanical properties of the substrate; h_p and h_{sub} are the thicknesses of the active layer and the substrate respectively. Thus, the effective piezoelectric coefficient in compression $d_{33_{eff}}$ is given by the following equation:

$$d_{33_{eff}} = d_{33} - 2d_{31}\frac{Y_p}{1-\nu_p}\left(\frac{h_p\left(1-\nu_{sub}\right)\nu_p + h_{sub}\left(1-\nu_p\right)\nu_{sub}}{h_p\left(1-\nu_{sub}\right)Y_p + h_{sub}\left(1-\nu_p\right)Y_{sub}} - \frac{\nu_p}{Y_p}\right) \tag{10}$$

Equation (10) shows that Y_{sub} and ν_{sub} are the key parameters to maximize $d_{33_{eff}}$ (in the absolute value). For an optimization, the following conditions must be met: ν_{sub} should be maximized and $Y_{sub} \ll Y_{PVDF}$, meaning that a flexible substrate is preferred to improve the effective d_{33}.

Although the thicknesses h_p and h_{sub} were set earlier to achieve good conformability, their values also strongly influence the model. To optimize sensor sensitivity, h_p must be minimized and h_{sub} maximized. The thickness of the piezoelectric film has already been minimized within the limits of what screen-printing allows. More interestingly, this shows that the choice of substrate thickness must be a compromise between device flexibility and performance.

Equation (10) also shows that $d_{33_{eff}}$ depends only on material parameters and is independent of the applied stress. Combined with Equation (2), this justifies the linearity between the piezoelectric response of the sensor and the applied compressive force, as observed in Figure 4c,d.

For numerical application, the mechanical properties of the substrates were taken from Table 1. Regarding the active layer, the values of d_{33} and d_{31} are of primary importance for the accuracy of the analytical model. Unfortunately, it is difficult to measure separately these parameters in practice, because of the mechanical interaction between the substrate and the active element which is ultimately multidirectional and strongly depends on the substrate's flexibility. Accordingly, d_{33} and d_{31} were adjusted within the interval found in the literature as follows:[69]

- $-35\ \text{pC.N}^{-1} \leq d_{33} \leq -25\ \text{pC.N}^{-1}$
- $10\ \text{pC.N}^{-1} \leq d_{31} \leq 20\ \text{pC.N}^{-1}$

Figure 5b compares the experimental measurements of $d_{33_{eff}}$ with the predictions made by the model. Small defects in the P(VDF-TrFE) active layer may explain the experimental variability observed between sensors. A good fit is confirmed for sensors on PI substrate. In this case, $Y_{sub} \approx Y_{PVDF}$, the d_{31} contribution tends toward 0, resulting in $d_{33_{eff}} \approx d_{33}$. The model also fits reasonably well for the TPU substrate, although $d_{33_{eff}}$ is measured experimentally higher than the model prediction. This discrepancy could be attributed to the actual complexity of the mechanical behavior of TPU, which is neither elastic nor isotropic.

To support and validate the experimental results as well as the analytical model, 2D FE numerical simulation on COMSOL Multiphysics was investigated. The same configuration as the one used for the model was adopted (Figure 5a), a force of 1 N was applied on a 5.3 mm^2 sensor. The thickness and the Poisson coefficient of the substrate were set as $h_{sub} = 100\ \mu\text{m}$ and $\nu_{sub} = 0.35$, while the Young's modulus Y_{sub} was varied between 10 MPa and 10 GPa. The simulation result of Figure 5c highlights that the in-plane strain distribution is homogeneous at the center of the

device in both active and substrate layers, as assumed for Equation (5). At the edge of the sensor, however, a local rebound effect with significantly higher strains (and higher stresses as well) is observed. Such an effect prevents direct comparison of the generated piezoelectric charge with the analytical model, which assumes the in-plan strain is uniform for all layers. In practice, this rebound effect is neither visible nor measurable, as the flat indenter impedes it, and the active layers of copolymer and PEDOT:PSS do not reach the edge of the device.

Figure 5d demonstrates that the average in-plane strain due to the Poisson effect in the simulation is correlated with the model's trend. Indeed, the analytical model estimates a strain ≈20–30% lower than the simulation's one, which is acceptable given the significant variation of the strain (more than a decade) over a large range of the Young's modulus of the substrate. The result also suggests that the substrate's flexibility does affect the deformation ability of the sensor, which in turn modifies its piezoelectric sensitivity. As lower Y_{sub} leads to higher strains (so higher $d_{33_{eff}}$), TPU is clearly preferred over its PI counterpart. Furthermore, there is no need to look for a softer substrate to further improve performance, as a plateau has been reached with TPU.

Overall, the theoretical model and numerical simulation are consistent with the empirical measurements. All results confirm the use of TPU for outstanding enhancement of the piezoelectric performance under compressive load due to the Poisson effect. The best approach for a conformable force sensor is to select a substrate with a Young's modulus significantly lower than that of the piezoelectric material. This way, Poisson's ratio deformation in the substrate creates additional stresses in the piezoelectric layer, considerably enhancing its compressive performance and the device's sensitivity. The choice of substrate based on its mechanical properties is a key factor for performance optimization. In the case of the comparison between TPU and PI substrates, the performance benefit provided by TPU more than compensates for the slight advantage in processability of PI. Therefore, in the next study, the characterization of the double-sided sensor only focuses on TPU substrate.

3.4. Mechanical Characterizations of the Double-Sided Sensor

Henceforth, D is considered as the mean signal of a double-sided device:

$$D = \frac{D_a + D_b}{2} \tag{11}$$

where D_a and D_b denote the electric displacement of the two individual sensors on both sides of the device. The working principle of a double-sided conformable piezoelectric sensor is illustrated in **Figure 6**a. For compression, the stress is uniformly transmitted to both sensors. Since dipole orientation and connection to the interface electronics are perfectly symmetrical, both sensors produce an identical signal ($D_a = D_b$). For bending, the sensors are perfectly symmetrical on each side of the neutral fiber. We can distinguish two types of stress that generate loads according to the d_{31} mode of piezoelectricity: in-plane traction (IPT) for the sensor outside the neutral fiber during bending and in-plane compression (IPC) for the one inside the neutral fiber (Figure 6b). Thus, by symmetry, both sensors are subjected to

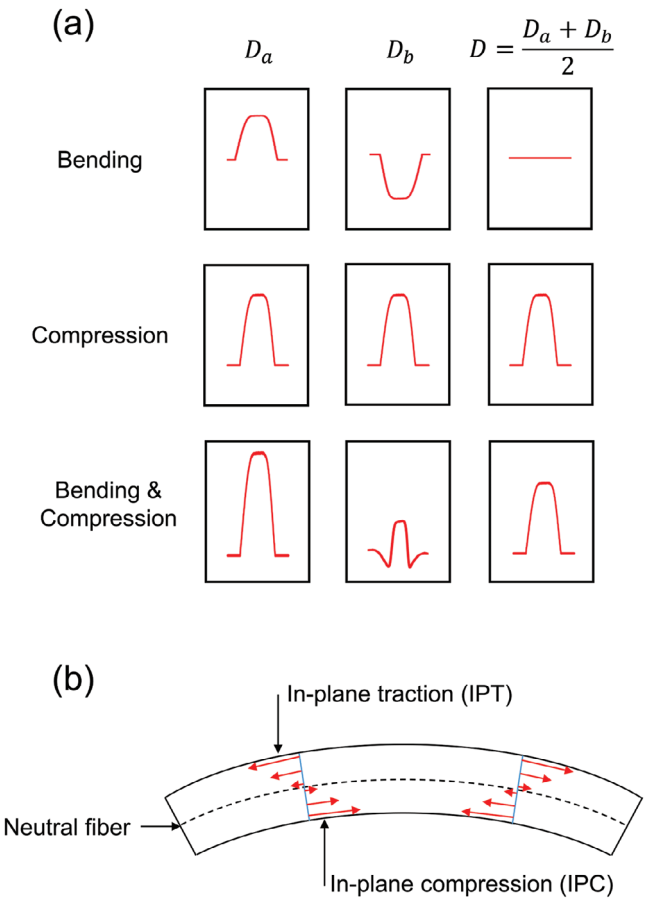

Figure 6. a) Working principle of a double-sided sensor to eliminate bending signal; b) difference between in-plane traction and in-plane compression during bending.

the same stress intensity, but with opposite sign ($D_a = -D_b$). When bending and compression occur simultaneously, each sensor generates a combined signal, but the bending component can be eliminated based on the post-processed mean signal D.

Obviously, this principle works regardless of the direction of polarization or the sensor connections. It only changes if the signals need to be added or subtracted to eliminate bending. To keep things simple, we will consistently use the configuration described above.

To completely overcome the bending effect, the two sensors of a bimorph must deliver perfectly opposite signals when bent overload. To verify this, the setup was slightly modified so that the double-sided device was positioned perpendicular to the surfaces of the glass support and the indenter, i.e., along the direction of motor's movement. The bending of the device occurred when the indenter pressed against its edge. Different bending amplitudes in both opposite bending directions were studied.

As illustrated in **Figure 7**a,b, the bending response of the two sensors on each side of the neutral fiber is not symmetrical, as the output responses D_a and D_b of the bimorph sensors are not perfectly opposite in practice. Thus, the mean charge D computed from Equation (11) allows for the elimination of ≈80% of the bending effect, even for bimorphs where the sensors have nearly

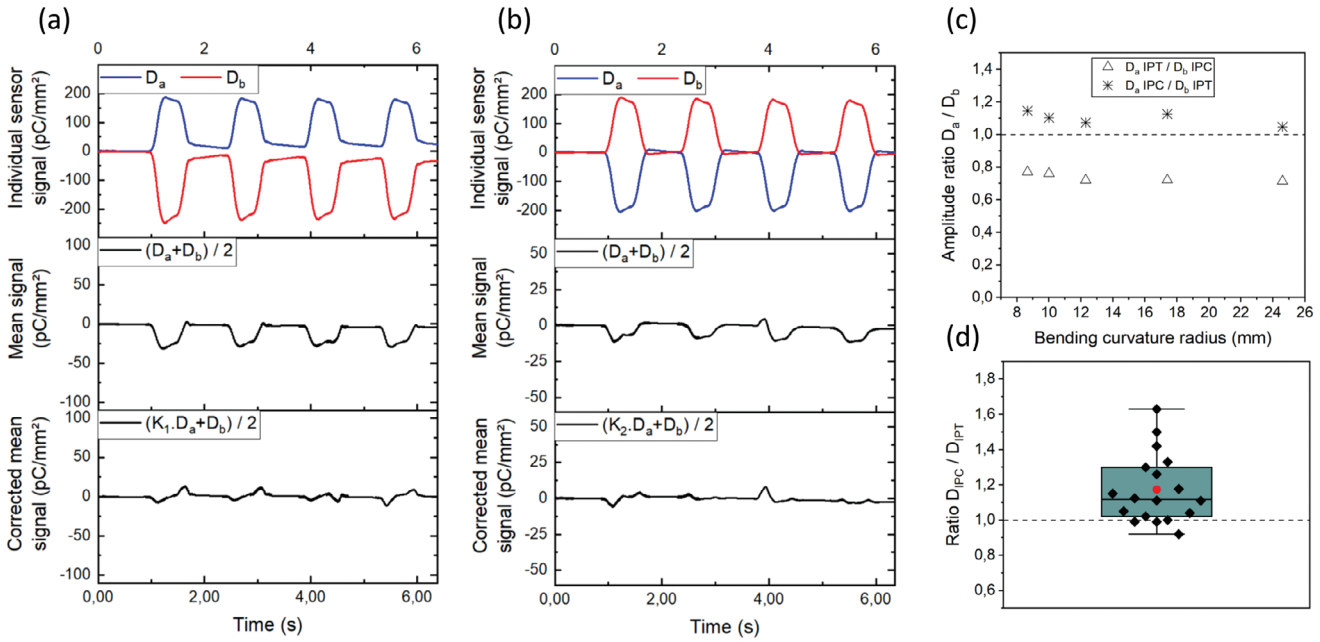

Figure 7. Characterization of double-sided sensors in bending: sensor response to bending a) in one direction, and b) in the opposite direction; c) bending asymmetry as a function of the curvature radius; d) ratio of signal for multiple bimorphs between the sensor with in-plane compression and the sensor with in-plane traction during bending. The subscripts in K_1 and K_2 differentiate the values of the corrective coefficient.

identical electrical characteristics. This asymmetry of the double-sided sensor, assessed by the ratio D_a/D_b, is globally constant regardless of the bending amplitude (Figure 7c). For all tested bimorphs with TPU substrate (Figure 7d), it was almost systematically the sensor inside the neutral fiber with IPC that generated a higher electric charge than the one outside of the neutral fiber with IPT. There were a few exceptions where one sensor of a bimorph was significantly more efficient than the other, so it generated a larger signal regardless of the bending direction.

Such a phenomenon probably originated from an asymmetric behavior of d_{31} coefficient whose value was found greater for IPC than for IPT. This effect, to some extent, has consequences for the use of conformable bimorphs to measure compressive forces. Since IPC (from bending) generates an electric charge opposite to that from out-of-plane compression (from compressive force), if the asymmetric bending effect is not corrected, the measured compressive force is always underestimated. It is also highlighted in Figure S3 (Supporting Information) that the asymmetric bending effect does not depend on the poling direction.

Since the asymmetry does not depend on the bending amplitude, a corrective coefficient K (the so-called weight factor) was applied to adjust D close to 0 under bending. Instead of using Equation (11), D can be corrected using the weighted average formula as follows:

$$D = \frac{K.D_a + D_b}{2} \tag{12}$$

K depends on which sensor is in IPC and which one is in IPT, meaning that the latter must be known before using the sensor in real application. Figure 7a,b shows that a slight bending interference signal still remains even with an optimized value of K. Nonetheless, the result is satisfactory with ≈95% of the bending effect rejected, allowing for accurate extraction of the output signal induced by the compressive load.

For practical applications, the users seek a value of K as close as possible to 1, regardless of the bending direction. In this case, a maximum of the bending signal is eliminated, even without the correction, and the uncertainty associated with the estimation of K can be ignored. As this coefficient appears intrinsically linked to the natural asymmetry of the piezoelectric material's behavior under bending conditions, the target value is likely unattainable, at least for P(VDF-TrFE). However, it is possible to approach $K = 1$ by minimizing other sources of asymmetry arising from the fabrication process. Piezoelectric films should be identical, with the same thickness and crystalline structure. It is therefore advisable to use materials and processes that are simple and repeatable, further supporting the advantages of using screen-printing and a P(VDF-TrFE) film in this study. In practice, the value of K generally varied within the range [0.7–1.3], as shown in Figure 7c,d.

Overall, a double-sided sensor needs a bending calibration to estimate the corrective coefficient K in both opposite bending directions and a compressive calibration to estimate the effective d_{33} of both sensors.

After these calibrations, the double-sided sensor was tested in a realistic situation where both bending and compression were applied simultaneously. Accordingly, the flat indenter was replaced by a curved one, and a foam support was used instead of the glass support. This configuration faithfully simulates real conditions in the medical field, e.g., measuring the pressure of a finger on human skin. The indenter applies a compressive force along the thickness direction, but the foam and the conformable sensor bend to match the shape of the curved indenter. Indenters with

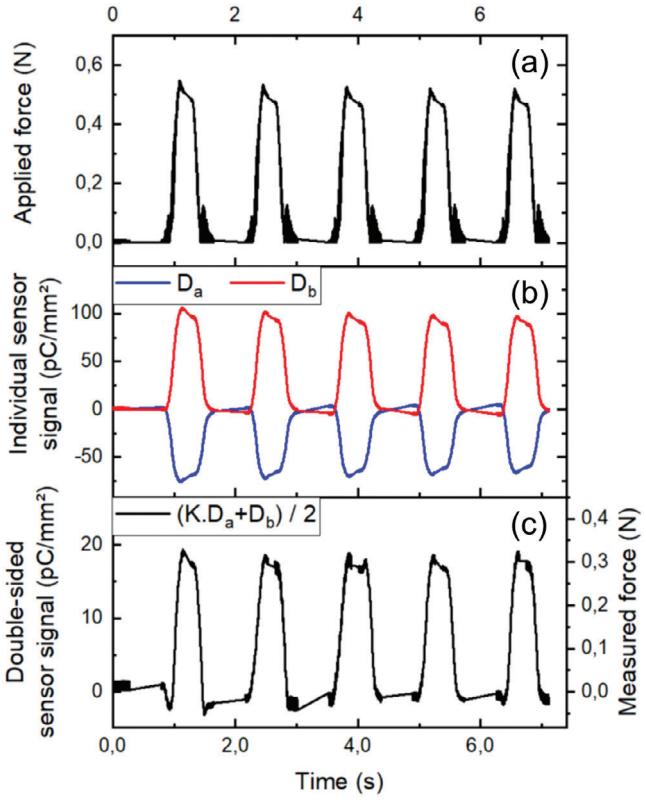

Figure 8. Signal of a double-sided sensor under combined bending and compressive stresses during pressure on a foam plate: a) force applied by the indenter; b) individual sensor responses; c) double-sided sensor response with the corrected mean signal.

a single axis of curvature with different curvature radius were tested, and the results are presented in **Figure 8**.

As shown in Figure 8b, even at low applied force, bending predominates over-compression in a bimorph, as evidenced by the opposite signals from the two sensors. However, when bending is compensated using Equation (12), the post-treated signal of the double-sided sensor (Figure 8c) is consistent with the applied compressive load (Figure 8a). Interestingly, the measured force deduced from the piezoelectric sensor ($F_{measured}$) is somewhat lower than the one given by the load cell ($F_{applied}$) integrated into the testbench. In practice, the contact surface between the sensor and the indenter (S_c) is larger than the effective surface of the sensor itself (S_{eff}, defined by the electrodes area), so the force ratio $F_{measured}/F_{applied}$ is always less than 1. As expected, increasing the applied force or the curvature radius of the indenter leads to an increase in S_c and as a result, a decrease in the ratio (see Figure S4, Supporting Information). Thus, it can be reasonably assumed that the sensor measured the actual force applied to its effective surface and the bending correction was successful.

For the piezoelectric bimorph principle to work properly, the double-sided sensor must conform to the surfaces it comes into contact with. For example, as the sensor is originally flat, it cannot fully conform to a spherical surface. When a double-sided sensor was pressed with a hemispherical indenter, inconsistencies were observed between the force applied and the force measured by the device (Figure S5, Supporting Information).

3.5. Applications in the Medical Fields

Many applications are foreseen in the medical field, either for fundamental science measurements (in vitro or ex vivo studies) or even for clinical applications. Numerous studies already confirmed the biocompatibility of the main materials used in this study such as PI, TPU, P(VDF-TrFE), and PEDOT:PSS.[46,72–75]

The sensors were tested in a complex environment to ensure their reliability for medical applications. They were plated at the bottom of a container filled with isotonic saline solution (distilled water with 0.9% sodium chloride), commonly used in healthcare due to its ionic concentration, which is identical to that of blood. The solution could be preheated on a hot plate, and its temperature was continuously monitored with a thermocouple. The sensors, immersed in saline solution, were tested with the pressure test bench presented in Figure 4a. The tests were performed at a constant temperature to ignore pyroelectric effects.

Figure 9a shows that at room temperature, immersion in saline solution has no significant influence on sensor performance. This is due to the effective encapsulation provided by non-active, hydrophobic P(VDF-TrFE). When the temperature is raised to body temperature (≈37 °C), a slight increase in $d_{33_{eff}}$ can be observed. This is consistent with an increase in the piezoelectric coefficients d_{31} and d_{33} of P(VDF-TrFE) with temperature as reported in the literature.[76] However, for such a small variation in temperature, the increase in sensitivity is marginal (only 10%), actually within the testbench's measurement uncertainty. This phenomenon can thus be ignored for the rest of the study.

The aging effect was tested by applying 1000 cycles at ≈200 kPa (1500 mmHg) at 1 Hz. These mechanical stresses are representative of the intended applications, with amplitudes even higher than those expected. The test was carried out at room temperature to easily maintain a stable temperature, and in saline solution to verify the durability of the encapsulation. Figure 9b shows that the sensor's sensitivity remains stable over 1000 cycles.

The developed device could first be used as a tactile sensor applied on human skin. Experiments on human subjects were performed with informed consent of the participants, who are the authors of this manuscript. Ethics committee approval was not required for these non-invasive measurements. As indicated in **Figure 10a**, the sensor was placed on the forearm and held in place by a film of paraffin; a force was applied by gently pressing with a finger. As shown in Figure 10b, opposing signals from the two sensors were observed, indicating a bending effect. After correction of the bending noise using Equation (12), the output signal was found to be consistent with a compression of a normal human touch (i.e., corresponding to a force of ≈0.3 N).

This demonstrates the potential of the device for precision tactile sensing, which is highly relevant for high-stakes applications such as human-machine interaction (HMI) or electronic skin (e-skin).[77] However, these applications require arrays with large surface areas and high sensor density. Regarding surface coverage, screen-printing is well-suited due to its speed and ability to process large print areas.[57] The primary technological challenge lies in the density of sensors and therefore the miniaturization of individual sensors. With sub-millimeter resolutions, screen-printing could theoretically be used to print sensors with a surface area in the range of $0.1 - 1$ mm^2. In practice, the main limitation would be the low capacitance of such sensors, whose

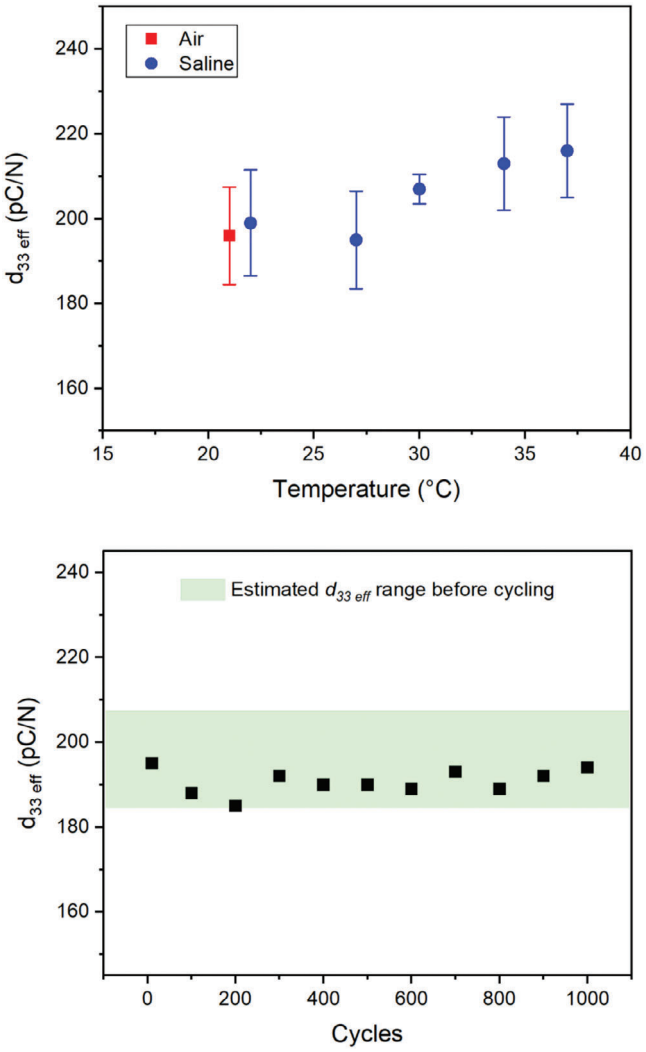

Figure 9. Reliability testing of a 4.15 mm^2 sensor in a complex environment representative of medical applications: a) effect of temperature and immersion in isotonic saline solution on sensor sensitivity; b) reliability over 1000 cycles at 200 kPa and 1 Hz in saline solution.

performance would be strongly impacted by the parasitic capacitances inherent to printed electronics. If the latter is estimated to range between 1 and 10 pF (due to high-density conductive tracks), a sensor would need a minimum capacitance of ≈50 pF, corresponding to a surface area of 2 mm^2 using a P(VDF-TrFE) layer with a thickness of 3 µm (which is already minimized). Such dimensions should be easily achievable by screen-printing with uniform layers stacked together. Consequently, all the performances obtained in this study should also applied to this small sensor. As reducing sensor surface area decreases its sensitivity, the increase in $d_{33_{eff}}$ thanks to a soft substrate should nonetheless enable pressure measurement in the 1–100 kPa range, which is of high interest for tactile sensing. All these considerations represent interesting perspectives for future studies.

Second, our development has a high potential for cardiovascular applications, specifically in the field of heart valves. Cardiac valves are actually made up of thin, flexible materials called leaflets. The contact between the leaflets provides a sealing mechanism ensuring the one-way valve function. The objective is to measure the contact forces between two valvular leaflets (known as coaptation forces) throughout the cardiac cycle. From a practical standpoint, determining such a physical quantity is challenging, yet of high interest for both intellectual and scientific purposes (better understanding of valve biomechanics) as well as for potential further clinical applications (intraoperative physical assessment to guide cardiac surgeries).[78,79]

As depicted in **Figure 11a**, the device was implemented in a cardiac valve testbench mimicking the behavior of a human mitral valve (BDC Laboratories, CO, USA). In this experimental setup, the valve was made of silicone, and the ventricle was made of rigid plastic. A pump circulates water to simulate realistic physiological parameters. The piezoelectric sensor was inserted into the system through the apex of the artificial heart (see Figure 11a,b). Figure 11c presents the output signals from the sensing device, which are once again primarily due to the bending effect. After data post-processing, the compression signal was isolated, allowing an estimation of the coaptation pressure at ≈60 kPa for a corresponding transmitral pressure of 170 mmHg. These findings are revealed to be consistent with those reported in the literature, confirming the reliability of the proposed sensing device.[80]

4. Conclusion

This study involved the development of a conformable piezoelectric sensor capable of measuring low compressive forces on non-flat or deformable surfaces. It has been revealed that the conformability between the sensing device and the contact surface (i.e., depending on their shape and stiffness) substantially impacts the sensor response. Consequently, theoretical models together with experimental characterizations were thoroughly investigated to better address this issue.

First, the choice of substrate, which determines the sensor's conformability, proved to be crucial due to its mechanical interaction with the piezoelectric film. Bending stiffness was considered a relevant criterion for substrate selection, and two approaches were explored to achieve good conformability: low thickness or low Young's modulus of the substrate. Based on the Poisson effect, a substrate with high flexibility relative to the active layer was preferred over a thin thickness. It has been demonstrated that a remarkable tenfold increase in the compression sensing performance was obtained with a flexible TPU substrate as opposed to a rigid PI, reaching efficiencies close to those of their rigid ceramic counterparts such as PZT. This finding opens up promising prospects for researching adequate substrate material as one of the key factors in optimizing the sensor response. A new analytical model was developed to estimate the effective piezoelectric coefficient in compression ($d_{33_{eff}}$) by considering the mechanical interaction between the active layer and the substrate. It is expected that the developed model could serve as a reference for substrate selection and device performance prediction.

Second, when the conformable sensor is subjected to a compressive force on a curved and/or deformable surface, a bending effect occurs that perturbs the sensing performance. Ideally, the output signal of the sensor should faithfully reflect the input compressive force. Hence, the bending signal must be eliminated

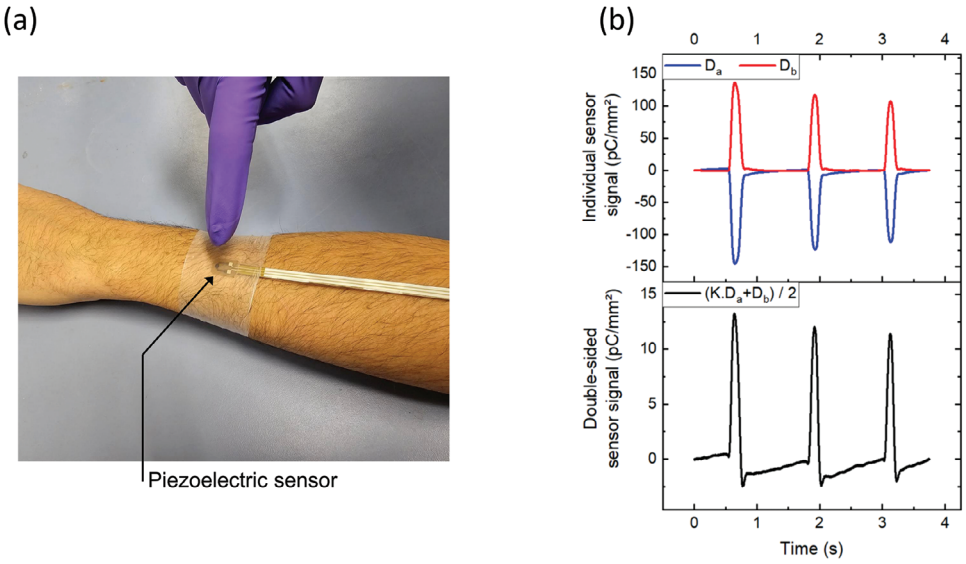

Figure 10. Application of the piezoelectric device for pressure measurement on skin: a) picture of the setup implemented on the forearms; b) output signals of unit sensors (top) and bimorph sensor (bottom).

to isolate the useful signal only. To achieve this, a double-sided structure was used to exploit the piezoelectric bimorph principle, wherein two opposite signals caused by bending are canceled out by averaging them. In practice, the bending effect, which depends on the bending direction and the sensor conformability, often predominates over the compression effect. Proper calibration and the application of corrective coefficients made it possible to successfully counterbalance the bending effect, which was essential for achieving an accurate output signal.

Finally, the challenges encountered in using the conformable device provide a foundation for future studies. The next logical step may involve studying the miniaturization of conformable sensors and their integration into piezoelectric arrays. This would enable high-precision pressure mapping on soft surfaces, opening up promising applications such as e-skin. It would also address the issue that a double-sided sensor subjected to several bending directions (e.g., if it is conformed to a wavy surface) does not function properly. Indeed, if an array were conformed to a wavy surface, locally each miniaturized sensor would likely be subjected to only a single bending direction. Research on arrays introduces new challenges, such as crosstalk reduction, optimal addressing of a large number of electrodes, and the development of new interface electronics capable of simultaneously processing the piezoelectric signals of numerous bimorphs set in an array. Regarding the non-conformability of flat sensors on spherical surfaces, it would be valuable to study whether the double-sided sensor concept could be combined with structural design to improve conformability.[81] As for future use of this sensor in medical applications, specific biocompatibility tests will need to be conducted on the device, as well as studies of sensor behavior and stability in an in vivo environment to ensure safety and reliability.

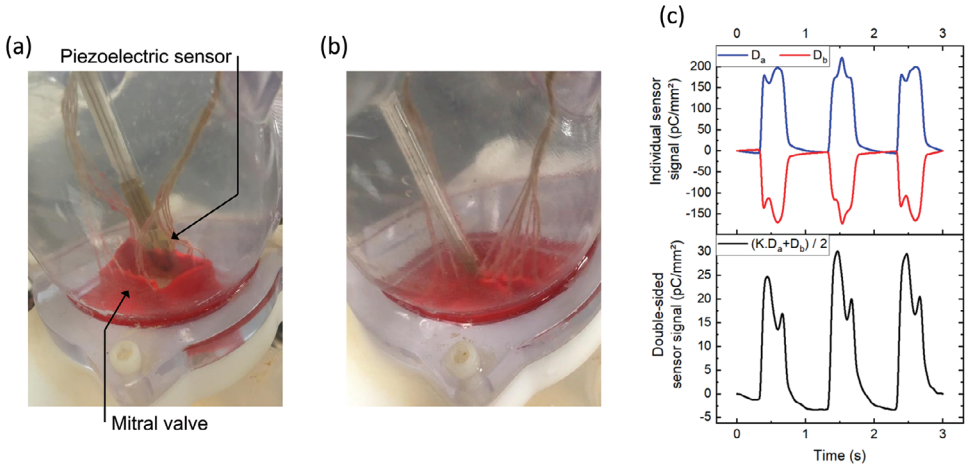

Figure 11. Application to the measurement of coaptation pressure in the mitral valve: a) double-sided piezoelectric sensor in (a) an open valve and b) a closed valve; c) output signals of unit sensors (top) and bimorph sensor (bottom).

Overall, this successful proof-of-concept for a piezoelectric conformable sensor developed in this study has paved the way for further explorations in medical instrumentation. The proposed sensor allows measurement of low coaptation forces in the mitral valve helping cardiac surgeons to better understand the biomechanics of this complex apparatus, marking an important first milestone.

Supporting Information

Supporting Information is available from the Wiley Online Library or from the author.

Acknowledgements

The authors would like to thank David Alincant for the fabrication of the sensors, Sylvain Minot and Sandrine Schlutig for DRX characterization, Yves Faucherand for SEM characterization, Laurent Tournon for sensor design and Arkema Piezotech for supplying the P(VDF-TrFE). Lastly, the authors also thank the ANR (French National Research Agency) with number ANR-22-CE09-0032-04 (IMINEN project) for partially financing some expenses throughout the research.This work wass principally supported by CEA (Commissariat à l'Energie Atomique et aux Energies Alternatives), France.

Conflict of Interest

The authors declare no conflict of interest.

Author Contributions

J.F. and M.-Q.L. wrote and edited the manuscript. J.F., M.B., and P.-J.C. performed experimental tests and interpreted the results. J.F. conducted theoretical models and plotted data. M.B. and J.F. designed and manufactured the samples. C.R. made XRD measurements and interpretations. A.A. carried out FE numerical simulations. D.G. defined specifications and validated the reality of the device. All authors have read and agreed to the published version of the manuscript.

Data Availability Statement

The data that support the findings of this study are available from the corresponding author upon reasonable request.

Keywords

bending effect, conformable sensors, ferroelectric polymer, medical applications, piezoelectric bimorphs

Received: June 7, 2024
Revised: October 29, 2024
Published online:

[1] A. B., S. Rao, H. J. Pandya, *Clin. Biomech.* **2019**, *69*, 127.
[2] G. Singh, A. Chanda, *Biomed. Mater. Bristol Engl.* **2021**, *16*, 062004.
[3] Y. Wu, Y. Ma, H. Zheng, S. Ramakrishna, *Mater. Des.* **2021**, *211*, 110164.
[4] S. Qian, L. Qin, J. He, N. Zhang, J. Qian, J. Mu, W. Geng, X. Hou, X. Chou, *Mater. Lett.* **2020**, *261*, 127119.
[5] Z. M. Tsikriteas, J. I. Roscow, C. R. Bowen, H. Khanbareh, *iScience* **2021**, *24*, 101987.
[6] W. Dong, L. Xiao, W. Hu, C. Zhu, Y. Huang, Z. Yin, *Trans. Inst. Meas. Control* **2017**, *39*, 398.
[7] Y. Du, R. Wang, M. Zeng, S. Xu, M. Saeidi-Javash, W. Wu, Y. Zhang, *Nano Energy* **2021**, *90*, 106522.
[8] J. Abanah Shirley, S. Esther Florence, B. S. Sreeja, R. Sankararajan, *Smart Mater. Struct.* **2022**, *31*, 125015.
[9] S. Y. Chung, H.-J. Lee, T. I. Lee, Y. S. Kim, *RSC Adv.* **2017**, *7*, 2520.
[10] H. B. Lee, Y. W. Kim, J. Yoon, N. K. Lee, S.-H. Park, *Smart Mater. Struct.* **2017**, *26*, 045032.
[11] S. V. Fernandez, F. Cai, S. Chen, E. Suh, J. Tiepelt, R. McIntosh, C. Marcus, D. Acosta, D. Mejorado, C. Dagdeviren, *ACS Biomater. Sci. Eng.* **2021**, *9*, 2070.
[12] K. L. Montero, M.-M. Laurila, M. Mäntysalo, in 2021 IEEE International Conference on Flexible and Printable Sensors and Systems (FLEPS), Manchester, United Kingdom, June **2021**, pp. 1–4.
[13] M. Wu, Y. Wang, S. Gao, R. Wang, C. Ma, Z. Tang, N. Bao, W. Wenxuan, F. Fan, W. Wu, *Nano Energy* **2019**, *56*, 693.
[14] R. Sun, S. C. Carreira, Y. Chen, C. Xiang, L. Xu, B. Zhang, M. Chen, I. Farrow, F. Scarpa, J. Rossiter, *Adv. Mater. Technol.* **2019**, *4*, 1900100.
[15] Z. Yi, Z. Liu, W. Li, T. Ruan, X. Chen, J. Liu, B. Yang, W. Zhang, *Adv. Mater.* **2022**, *34*, 2110291.
[16] L. Natta, F. Guido, L. Algieri, V. M. Mastronardi, F. Rizzi, E. Scarpa, A. Qualtieri, M. T. Todaro, V. Sallustio, M. De Vittorio, *ACS Sens.* **2021**, *6*, 1761.
[17] Y. Yuan, H. Chen, H. Xu, Y. Jin, G. Chen, W. Zheng, W. Wang, Y. Wang, L. Gao, *Sens. Actuators Phys.* **2022**, *345*, 113818.
[18] G. D'Ambrogio, O. Zahhaf, M.-Q. Le, M. Bordet, P. Lermusiaux, N. Della Schiava, R. Liang, P.-J. Cottinet, J.-F. Capsal, *Mater. Des.* **2022**, *223*, 111195.
[19] G. D'Ambrogio, O. Zahhaf, M. Bordet, M. Q. Le, N. Della Schiava, R. Liang, P.-J. Cottinet, J.-F. Capsal, *Adv. Eng. Mater.* **2021**, *23*, 2100341.
[20] M. Cheng, G. Zhu, F. Zhang, W. Tang, S. Jianping, J. Yang, L. Zhu, *J. Adv. Res.* **2020**, *26*, 53.
[21] E. Elnabawy, A. H. Hassanain, N. Shehata, A. Popelka, R. Nair, S. Yousef, I. Kandas, *Polymers* **2019**, *11*, 1634.
[22] N. Amiri, F. Tasnim, M. T. Anbarani, C. Dagdeviren, M. A. Karami, *Smart Mater. Struct.* **2021**, *30*, 085017.
[23] C. Dagdeviren, Y. Shi, P. Joe, R. Ghaffari, G. Balooch, K. Usgaonkar, O. Gur, P. L. Tran, J. R. Crosby, M. Meyer, Y. Su, R. Chad Webb, A. S. Tedesco, M. J. Slepian, Y. Huang, J. A. Rogers, *Nat. Mater.* **2015**, *14*, 728.
[24] X. Zhang, M.-Q. Le, V.-C. Nguyen, J.-F. Mogniotte, J.-F. Capsal, D. Grinberg, P.-J. Cottinet, L. Petit, *Mater. Des.* **2021**, *208*, 109912.
[25] W.-S. Jung, M.-J. Lee, M.-G. Kang, H. G. Moon, S.-J. Yoon, S.-H. Baek, C.-Y. Kang, *Nano Energy* **2015**, *13*, 174.
[26] X. Yuan, X. Gao, J. Yang, X. Shen, Z. Li, S. You, Z. Wang, S. Dong, *Energy Environ. Sci.* **2020**, *13*, 152.
[27] M.-S. Kim, H.-R. Ahn, S. Lee, C. Kim, Y.-J. Kim, *Sens. Actuators Phys.* **2014**, *212*, 151.
[28] A. Barzegar, D. Damjanovic, N. Ledermann, P. Muralt, *J. Appl. Phys.* **2003**, *93*, 4756.
[29] H. Fares, Y. Abbass, M. Valle, L. Seminara, *Sensors* **2020**, *20*, 1160.
[30] W. Lin, B. Wang, G. Peng, Y. Shan, H. Hu, Z. Yang, *Adv. Sci.* **2021**, *8*, 2002817.
[31] C. Mo, J. Davidson, W. W. Clark, *Smart Mater. Struct.* **2014**, *23*, 045005.

[32] C. Dagdeviren, Y. Su, P. Joe, R. Yona, Y. Liu, Y.-S. Kim, Y. Huang, A. R. Damadoran, J. Xia, L. W. Martin, Y. Huang, J. A. Rogers, *Nat. Commun.* **2014**, *5*, 4496.
[33] N. Chakhchaoui, H. Jaouani, R. Farhan, A. Eddiai, M. Meddad, O. Cherkaoui, L. V. Langenhove, *IOP Conf. Ser. Mater. Sci. Eng.* **2020**, *827*, 012046.
[34] A. B. Dobrucki, P. Pruchnicki, *Sens. Actuators Phys.* **1997**, *58*, 203.
[35] A. Fernandes, J. Pouget, *Int. J. Solids Struct.* **2003**, *40*, 4331.
[36] D. Benasciutti, L. Moro, S. Zelenika, E. Brusa, *Microsyst. Technol.* **2010**, *16*, 657.
[37] Y. Hong, B. Wang, W. Lin, L. Jin, S. Liu, X. Luo, J. Pan, W. Wang, Z. Yang, *Sci. Adv.* **2021**, *7*, eabf0795.
[38] E. S. Nour, C. O. Chey, M. Willander, O. Nur, *Nanotechnology* **2015**, *26*, 095502.
[39] D.-M. Shin, E. Tsege, S. Kang, W. Seung, S.-W. Kim, H. Kim, S. W. Hong, Y.-H. Hwang, *Nano Energy* **2015**, *12*,.
[40] D.-Y. Jung, S.-H. Baek, M. R. Hasan, I.-K. Park, *J. Alloys Compd.* **2015**, *641*, 163.
[41] B. Gil, B. Li, A. Gao, G.-Z. Yang, *ACS Appl. Electron. Mater.* **2020**, *2*, 2669.
[42] T. Sharma, K. Aroom, S. Naik, B. Gill, J. X. J. Zhang, *Ann. Biomed. Eng.* **2013**, *41*, 744.
[43] Z. Pi, J. Zhang, C. Wen, Z. Zhang, D. Wu, *Nano Energy* **2014**, *7*, 33.
[44] X. Chen, X. Han, Q.-D. Shen, *Adv. Electron. Mater.* **2017**, *3*, 1600460.
[45] S. Sukumaran, S. Chatbouri, D. Rouxel, E. Tisserand, F. Thiebaud, T. B. Zineb, *J. Intell. Mater. Syst. Struct.* **2021**, *32*, 746.
[46] Y. Kondo, S. Horike, Y. Koshiba, T. Fukushima, K. Ishida, *Jpn. J. Appl. Phys.* **2020**, *59*, SDDF02.
[47] S. Azimi, A. Golabchi, A. Nekookar, S. Rabbani, M. H. Amiri, K. Asadi, M. M. Abolhasani, *Nano Energy* **2021**, *83*, 105781.
[48] M.-H. You, X.-X. Wang, X. Yan, J. Zhang, W.-Z. Song, M. Yu, Z.-Y. Fan, S. Ramakrishna, Y.-Z. Long, *J. Mater. Chem. A* **2018**, *6*, 3500.
[49] P. Yu, W. Liu, C. Gu, X. Cheng, X. Fu, *Sensors* **2016**, *16*, 819.
[50] L. Persano, C. Dagdeviren, Y. Su, Y. Zhang, S. Girardo, D. Pisignano, Y. Huang, J. A. Rogers, *Nat. Commun.* **2013**, *4*, 1633.
[51] H. Abdolmaleki, A. B. Haugen, K. B. Buhl, K. Daasbjerg, S. Agarwala, *Adv. Sci.* **2023**, *10*, 2205942.
[52] S. Kim, I. Towfeeq, Y. Dong, S. Gorman, A. M. Rao, G. Koley, *Appl. Sci.* **2018**, *8*, 213.
[53] J. Polasik, V. Schmidt, *Proc. SPIE – Int. Soc. Opt. Eng* **2005**, *5759*, 114.
[54] X. Qiu, A. J. Benjamin, T. R. Venkatesan, G. C. Schmidt, R. A. Q. Soler, P. M. Panicker, R. Gerhard, A. C. Hübler, *IEEE Trans. Dielectr. Electr. Insul.* **2020**, *27*, 1683.
[55] B. Li, C. Cai, Y. Liu, F. Wang, B. Yang, Q. Li, P. Zhang, B. Deng, P. Hou, W. Liu, *Nat. Commun.* **2023**, *14*, 4000.
[56] J. Faudou, R. Ramos, M. Benwadih, *Adv. Mater. Technol.* **2023**, *8*, 2201495.
[57] M. Aliqué, C. D. Simão, G. Murillo, A. Moya, *Adv. Mater. Technol.* **2021**, *6*, 2001020.
[58] J. Wiklund, A. Karakoç, T. Palko, H. Yiğitler, K. Ruttik, R. Jäntti, J. Paltakari, *J. Manuf. Mater. Process.* **2021**, *5*, 89.
[59] C. Carbone, M. Benwadih, G. D'Ambrogio, M.-Q. Le, J.-F. Capsal, P.-J. Cottinet, *Polymers* **2021**, *13*, 2166.
[60] S. Toinet, M. Benwadih, H. Szambolics, C. Revenant, D. Alincant, M. Bordet, J.-F. Capsal, N. Della-Schiava, M.-Q. Le, P.-J. Cottinet, *Materials* **2024**, *17*, 2135.
[61] V.-C. Nguyen, M.-Q. Le, S. Bernadet, Y. Hebrard, J.-F. Mogniotte, J.-F. Capsal, P.-J. Cottinet, *Polymers* **2023**, *15*, 826.
[62] M. Kuş, S. Okur, *Sens. Actuators, B* **2009**, *143*, 177.
[63] C. Mo, L. J. Radziemski, W. W. Clark, *Smart Mater. Struct.* **2010**, *19*, 025016.
[64] S. Toinet, M. Benwadih, S. Tardif, J. Eymery, C. Revenant, *J. Polym. Res.* **2022**, *29*, 456.
[65] T. Furukawa, *IEEE Trans. Electr. Insul.* **1989**, *24*, 375.
[66] F. Pedroli, A. Marrani, M.-Q. Le, C. Froidefond, P.-J. Cottinet, J.-F. Capsal, *J. Polym. Sci. Part B Polym. Phys.* **2018**, *56*, 1164.
[67] C. Chen, S. Zhao, C. Pan, Y. Zi, F. Wang, C. Yang, Z. L. Wang, *Nat. Commun.* **2022**, *13*, 1391.
[68] J. Yang, *An Introduction to the Theory of Piezoelectricity*, Kluwer Academic Publishers, Boston, **2005**.
[69] B. Stadlober, M. Zirkl, M. Irimia-Vladu, *Chem. Soc. Rev.* **2019**, *48*, 1787.
[70] R. N. Torah, S. P. Beeby, N. M. White, *J. Phys. Appl. Phys.* **2004**, *37*, 1074.
[71] Y. Luo, *Materials* **2022**, *15*, 5656.
[72] C. Boehler, Z. Aqrawe, M. Asplund, *Bioelectron. Med.* **2019**, *2*, 89.
[73] L. Poole-Warren, P. Martens, R. Catani, *Biosynthetic Polymers for Medical Applications* **2016**.
[74] C. P. Constantin, M. Aflori, R. F. Damian, R. D. Rusu, *Materials* **2019**, *12*, 3166.
[75] N. Della Schiava, F. Pedroli, K. Thetpraphi, A. Flocchini, M.-Q. Le, P. Lermusiaux, J.-F. Capsal, P.-J. Cottinet, *Sci. Rep.* **2020**, *10*, 8805.
[76] K. Omote, H. Ohigashi, K. Koga, *J. Appl. Phys.* **1997**, *81*, 2760.
[77] X. Wang, L. Dong, H. Zhang, R. Yu, C. Pan, Z. L. Wang, *Adv. Sci.* **2015**, *2*, 1500169.
[78] D. Grinberg, M.-Q. Le, Y. J. Kwon, M. A. Fernandez, D. Audigier, F. Ganet, J.-F. Capsal, J. F. Obadia, P.-J. Cottinet, *Sci. Rep.* **2019**, *9*, 4677.
[79] M. P. Sá, X. Jacquemyn, J. V. den Eynde, O. Erten, T. Caldonazo, T. Doenst, M. Marin-Cuartas, M. A. Borger, M.-A. Clavel, P. Pibarot, R. Rodriguez, B. Ramlawi, S. Goldman, *Struct. Heart* **2023**, *7*, 100152.
[80] J. Adams, M. J. O'Rourke, *J. Biomech. Eng.* **2015**, *137*, 071008.
[81] C. Wang, C. Wang, Z. Huang, S. Xu, *Adv. Mater.* **2018**, *30*, 1801368.